UNIVERSIDAD DE CONCEPCIÓN
FACULTAD DE CIENCIAS FÍSICAS Y MATEMÁTICAS

(Quasi-)normal modes of rotating black holes and solitons in Einstein-Gauss-Bonnet

Por: Lilianne Febe Tapia Pérez

Tesis presentada a la Facultad de Ciencias Físicas y Matemáticas de la Universidad de Concepción para optar al grado académico de Magíster en Ciencias con Mención en Física

Marzo 2025
Concepción, Chile

Profesor Guía: Julio Oliva Zapata

A mi familia.

AGRADECIMIENTOS

A lo largo de estos años de estudio, he tenido la oportunidad de conocer y compartir con personas que han sido parte importante en este proceso, de las cuales me encuentro profundamente agradecida.

Gracias a los profesores por cada clase y a los compañeros con quienes compartí este camino. Estoy muy agradecida por el aprendizaje, el apoyo mutuo y las conexiones que formamos a lo largo de este proceso.

Quiero expresar mi sincero agradecimiento a mi grupo de amigos, con quienes vivimos momentos inolvidables, risas y profundas conversaciones que me enriquecieron tanto a nivel personal como académico. También quiero agradecer a quienes tuve la oportunidad de conocer y compartir en la sala de Postgrado, por el ambiente de compañerismo y los consejos compartidos.

Quiero extender un agradecimiento especial a mi profesor guía. por su paciencia infinita, su orientación precisa y buena disposición. Su ejemplo de dedicación y profesionalismo será una referencia para mí a lo largo de mi vida.

No puedo dejar de agradecer a mi familia, quienes han sido mi refugio incondicional. Su apoyo, paciencia y amor han sido fundamentales. Finalmente, gracias a Dios por iniciar este camino y terminarlo, por su cálida compañía en todo momento de este proceso, por las personas que pude conocer y las experiencias que me permitió vivir.

Resumen

Los parámetros que caracterizan cada espaciotiempo pueden influir directamente en el comportamiento de los modos cuasinormales. El análisis que se presentará comienza con el agujero negro de Bañados-Teitelboim-Zanelli (BTZ), una geometría en la que las frecuencias pueden calcularse analíticamente. A continuación, se aborda el agujero negro de Schwarzschild Anti-de Sitter (AdS), cuyo estudio requiere el uso de métodos numéricos. Finalmente, se investigan geometrías donde los modos no han sido explorados, específicamente soluciones a la teoría de Einstein-Gauss-Bonnet en el punto de Chern-Simons en cinco dimensiones.

En los resultados nuevos se consideran campos escalares sin masa para obtener las frecuencias sobre geometrías de solitones estáticos y agujeros negros rotantes. Estas se caracterizan por el momento angular j, la masa M y un parámetro de origen gravitacional b. El análisis se centra en el comportamiento de los modos como función del tamaño del solitón r_0, junto con los parámetros j y b.

Comenzando por los solitones, se observa un comportamiento monótono de los modos normales a medida que b aumenta desde cero, mientras que ocurre una anomalía cuando r_0 toma valores muy pequeños. Por otro lado, en el caso de los agujeros negros, se identifica una bifurcación en las frecuencias fundamentales al alcanzar un valor crítico del parámetro b. Además, al estudiar la variación de j, se distingue la existencia de dos ramas: una co-rotante y otra contra-rotante. Cada rama se identifica según su relación con el momento angular n del campo escalar.

Abstract

The parameters that characterize each spacetime can directly influence the behavior of the quasi-normal modes. The analysis to be presented begins with the static BTZ black hole, a geometry in which frequencies can be calculated analytically. The Schwarzschild-AdS black hole is then discussed, whose study requires the use of numerical methods. Finally, geometries where the modes have not been explored are investigated, in particular solutions to the Einstein-Gauss-Bonnet theory at the Chern-Simons point in five dimensions.

In the new results, massless scalar fields are considered to obtain the frequencies over static soliton and rotating black hole geometries. These are characterized by the angular momentum j, the mass M and a gravitational origin parameter b. The analysis focuses on the behavior of the modes as a function of the soliton size r_0, along with the parameters j and b.

Starting with solitons, a monotonic behavior of the normal modes is observed as b increases from zero, while an anomaly occurs when r_0 takes small values. On the other hand, in the case of black holes, a bifurcation in the fundamental frequencies is identified when reaching a critical value of the parameter b. Furthermore, when studying the variation of j, the existence of two branches is distinguished: one co-rotating and the other counter-rotating. Each branch is identified according to its relation to the angular momentum n of the scalar field.

Contents

List of Figures

Chapter 1

Introduction

Black holes are widely studied objects and of great interest in physics; they are known to be part of the universe because observational evidence confirms their existence. Real images of M87* and Sgr A* have been captured thanks to the collaboration of the Event Horizon Telescope (EHT). Additionally, black hole mergers, which generate spacetime vibrations detectable as gravitational waves, have been observed using the Laser Interferometer Gravitational-Wave Observatory (LIGO) and Virgo detectors [1].

Spacetime vibrations occur when black holes are perturbed, and these can be understood by drawing an analogy to the vibrations of a guitar string, which oscillates like sound waves until its energy dissipates. With this idea in mind, it is interesting to study how these frequencies, resulting from perturbations, behave. In some geometries these frequencies have only a real part, known as normal modes, while in others they include an imaginary component, indicating damping and are called quasi-normal modes.

There are several ways to calculate these frequencies, where the choice of method depends on the complexity of the differential equation to be solved. The first step involves identifying the geometry of interest, as this establishes the background for the analysis. The wave equation, formulated in terms of the metric defining the spacetime, is then employed. This setup provides the foundation for the study, after which it is necessary to specify what will be perturbed in this context. In this work, the analysis focuses on scalar field perturbations, allowing for the exploration of their interaction with the parameters of each geometry.

An interesting initial case to consider is the static BTZ (Bañados-Teitelboim-Zanelli) black hole [2] in three dimensions, which is a solution to Einstein's equations with a negative cosmological constant. The quasi-normal modes for this geometry can be calculated using analytical methods, and the properties of the Hypergeometric function [3] prove particularly useful for this purpose. The properties of the Hypergeometric function simplify the differential equation, making the structure of the solution more apparent. Furthermore, it is essential to work with the Gamma function, as it arises in the connection formulas for the Hypergeometric functions. A detailed examination of this case is presented in Chapter 2.

The analysis then progresses to the four-dimensional Schwarzschild-AdS black hole [4], which is also a solution to Einstein's equations with a negative cosmological constant. For this case, numerical methods are required to solve the resulting differential equation. The Frobenius method is employed to find first-order solutions near the horizon, providing an initial insight into the structure of the solution. The complete solution is then obtained using a power series approximation and numerical integration, with Mathematica being utilized for these calculations, as detailed in Chapter 3.

The quasi-normal modes mentioned above have been extensively studied, and their results are well documented in the literature. This allows for a comparison with the development used and to validate the numerical methods employed.

The primary objective is to calculate frequencies in spacetimes where novel results can be obtained. In particular, Chapter 4 focuses on the Einstein-Gauss-Bonnet theory at the Chern-Simons point [5], detailing the calculation of normal modes for static solitons and quasi-normal modes for rotating black holes. These studies explore the effects of varying parameters characterizing the geometry, such as the soliton size r_0, angular momentum j, and a gravitational hair parameter denoted by b.

Finally, comments and conclusions regarding the findings of this work are presented in Chapter 5

Chapter 2

Static BTZ black hole

An interesting geometry when starting to calculate quasi-normal modes is that of the static BTZ black hole [2], for which analytical methods can be employed. The metric that characterizes this spacetime is

$$ds^2 = -f(r)dt^2 + \frac{dr^2}{f(r)} + r^2 d\phi^2. \tag{2.0.1}$$

The domain of the coordinates is delimited by $-\infty < t < +\infty$, $r_+ < r < +\infty$ and $0 \leq \phi < 2\pi$ identified. Additionally, the function $f(r)$ is defined by

$$f(r) = r^2 - r_+^2, \tag{2.0.2}$$

considering the value of the AdS radius equal to one. This is a solution of Einstein equations with negative cosmological constant in $2+1$ dimensions, namely it solves

$$G_{\mu\nu} + \Lambda g_{\mu\nu} = 0 \tag{2.0.3}$$

with $\Lambda = -1$.

The interest in studying this geometry lies in the fact that is a simple model to work with, in which quasi-normal modes can be calculated analytically, results that have been previously obtained and that can be found in the literature, allowing comparison to ensure the effectiveness of the methods used.

To get into the topic, let us consider the equation for a massless scalar probe

$$\Box\Phi = 0, \tag{2.0.4}$$

which can be expressed in terms of the metric as:

$$\frac{1}{\sqrt{-g}}\partial_\mu\left(\sqrt{-g}g^{\mu\nu}\partial_\nu\Phi\right) = 0. \tag{2.0.5}$$

Utilizing equation (2.0.5) in conjunction with metric (2.0.1) results in

$$\frac{1}{r}\partial_t\left(\frac{r}{-f(r)}\partial_t\Phi\right) + \frac{1}{r}\partial_r\left(rf(r)\partial_r\Phi\right) + \frac{1}{r}\partial_\phi\left(\frac{1}{r}\partial_\phi\Phi\right) = 0, \tag{2.0.6}$$

where on purpose we have not provided further simplifications, for pedagogical reason.

Let us consider the following separation ansatz for the solution

$$\Phi(t,r,\phi) = \mathrm{Re}\left(\sum_{n=0}^{\infty}\int_{-\infty}^{\infty} d\omega e^{-i\omega t}e^{im\phi}R_{\omega,m}(r)\right), \tag{2.0.7}$$

here $m = 0, \pm1, \pm2, \ldots$. Then, it is possible to write (2.0.6) as

$$\left(\frac{\omega^2}{f(r)} - \frac{m^2}{r^2}\right)R(r) + \left(\frac{f(r)}{r} + f'(r)\right)R'(r) + f(r)R''(r) = 0, \tag{2.0.8}$$

and replacing $f(r) = r^2 - r_+^2$

$$\left(\frac{\omega^2}{r^2 - r_+^2} - \frac{m^2}{r^2}\right)R(r) + \left(3r - \frac{r_+^2}{r}\right)R'(r) + (r^2 - r_+^2)R''(r) = 0. \tag{2.0.9}$$

Solving the differential equation for the radial part is more convenient by making the following change of variable

$$x = 1 - \frac{r_+^2}{r^2}, \tag{2.0.10}$$

where the new domain is defined as $0 < x < 1$. In this way, equation (2.0.9) can be written as follows

$$x(1-x)R''(x) + (1-x)R'(x) + \frac{1}{4}\left(\frac{\omega^2}{xr_+^2} - \frac{m^2}{r_+^2}\right)R(x) = 0. \tag{2.0.11}$$

This is the resulting equation that we will solve analytically first, and then verify using the numerical method by comparing both results, to validate the correctness of the latter.

2.1 Analytical quasi-normal modes of BTZ black hole

The second order differential equation (2.0.11) can be solved by analytical method. Note that it closely resembles the form of the Hypergeometric equation [3]

$$x(1-x)F'' + [c-(a+b+1)x]F' - abF = 0, \tag{2.1.1}$$

for $F(x)$, when $R(x)$ is defined in the form

$$R(x) = x^{-\frac{\omega}{2r_+}i}(1-x)F(x). \tag{2.1.2}$$

Therefore, the solution of (2.1.1) reads

$$\begin{aligned} R(x) = {} & C_1 x^{-\frac{\omega}{2r_+}i}(1-x)\ {}_2F_1\left(1-\frac{\omega+m}{2r_+}i, 1-\frac{\omega-m}{2r_+}i, 1-\frac{\omega}{r_+}i, x\right) \\ & + C_2 x^{\frac{\omega}{2r_+}i}(1-x)\ {}_2F_1\left(1+\frac{\omega+m}{2r_+}i, 1-\frac{m-\omega}{2r_+}i, 1+\frac{\omega}{r_+}i, x\right). \end{aligned} \tag{2.1.3}$$

The next step is to analyze the boundary condition near the event horizon located at $x=0$. The property of the Hypergeometric function presented below will be used

$${}_2F_1(a,b,c,0) = 1. \tag{2.1.4}$$

Therefore, when $x \to 0$ (2.1.3) reduces to:

$$R(x) = C_1 x^{-\frac{\omega}{2r_+}i}(1-x) + C_2 x^{\frac{\omega}{2r_+}i}(1-x). \tag{2.1.5}$$

Focusing solely on the ingoing term, which in this instance corresponds to the negative exponent we derive the following expression for the solution

$$R(x) = C_1 x^{-\frac{\omega}{2r_+}i}(1-x)\ {}_2F_1\left(1-\frac{\omega+m}{2r_+}i, 1-\frac{\omega-m}{2r_+}i, 1-\frac{\omega}{r_+}i, x\right), \tag{2.1.6}$$

which fulfills ingoing boundary condition at the horizon.

Now, let us consider the boundary at infinite, $x \to 1$. Each term behaves in a controlled manner except for the Hypergeometric function, where it is not clear what is happening to it at first glance. The Kummer identity is useful for rewriting the function (2.1.6)

$$\begin{aligned} {}_2F_1(a,b,c,x) = &\frac{\Gamma(c)\Gamma(c-a-b)}{\Gamma(b-a)\Gamma(c-b)}\ {}_2F_1(a,b,+a+b-c-1,1-x) \\ &+\ {}_2F_1(c-a,c-b,1-a-b+c,1-x) \\ &\times\ \frac{\Gamma(c)\Gamma(a+b-c)}{\Gamma(a)\Gamma(b)}(1-x)^{c-a-b}. \end{aligned} \tag{2.1.7}$$

It is now possible to analyze the behavior when $x \to 1$. Observe that the values for a, b and c are

$$a = 1 - \frac{m+\omega}{2r_+}i, \tag{2.1.8}$$

$$b = 1 - \frac{m-\omega}{2r_+}i, \tag{2.1.9}$$

$$c = 1 - \frac{\omega}{r_+}i. \tag{2.1.10}$$

Therefore, using the property of Hypergeometric functions (2.1.4), writing (2.1.6) as

$$\begin{aligned} R(x) = &C_1 x^{-\frac{\omega}{2r_+}i}(1-x)\frac{\Gamma(c)\Gamma(c-a-b)}{\Gamma(b-a)\Gamma(c-b)} \\ &+ C_1 x^{-\frac{\omega}{2r_+}i}(1-x)\frac{\Gamma(c)\Gamma(a+b-c)}{\Gamma(a)\Gamma(b)}(1-x)^{c-a-b}, \end{aligned} \tag{2.1.11}$$

clearly captures the behavior as $x \to 1$.

The field does not vanish at infinity for the second term of (2.1.11), since the exponent of $(1-x)$, which is $c-a-b+1$, becomes zero, causing such term to tend to a constant as $x \to 1$. To ensure that the field cancels at infinity, it is necessary to cancel the second term of the equation $R(x)$, imposing

$$a = -p \quad \text{or} \quad b = -q, \tag{2.1.12}$$

with $p, q = 0, 1, 2, ...$, since the relevant Gamma functions diverge in that case.

From this it is possible to quantize the frequencies. Using the expressions (2.1.8) and (2.1.9), solving for ω gives

$$\omega = -\, m - 2r_+(1+p)i, \tag{2.1.13}$$
$$\omega = +\, m - 2r_+(1+q)i. \tag{2.1.14}$$

Note that the frequencies have a real and imaginary part. The latter is negative, therefore the scalar oscillations are indeed damped. We further identify m which corresponds to the angular momentum of the scalar field, while p and q represent the overtones.

2.2 Numerical quasi-normal modes of BTZ black hole

In the equation (2.0.11) the behavior is asymptotic at the extremes, near the horizon and as on approaches infinity. Studying the differential equation with the Frobenius method to leading order near $x = 0$, leads to the result

$$R(x) = C_1 x^{\frac{\omega}{2r_+}i}(1 + \mathcal{O}(x)) + C_2 x^{-\frac{\omega}{2r_+}i}(1 + \mathcal{O}(x)). \tag{2.2.1}$$

It is necessary to choose one of both roots by imposing the boundary condition at $x = 0$, which is the event horizon. Then multiplying (2.2.1) by the time dependence, leads to

$$e^{(-i\omega t)}R(x) = C_1 e^{-\left(i\omega t - \frac{i\omega}{2r_+}\ln(x)\right)} + C_2 e^{-\left(i\omega t + \frac{i\omega}{2r_+}\ln(x)\right)}. \tag{2.2.2}$$

This allows us to notice that the outgoing wave agrees with the first term and the ingoing with the second. Thus, retaining the second term and renaming constant C_2 as C, we propose

$$R(x) = Cx^{-\frac{\omega}{2r_+}i}F(x), \tag{2.2.3}$$

where the function has the behavior $F(x) = (1+\mathcal{O}(x))$. So, replacing that solution into equation (2.0.11) gives

$$x(1-x)F''(x) + (1-x)\left(1 - \frac{\omega}{r_+}i\right)F'(x) + \left[\left(\frac{\omega^2}{4r_+^2 x}(r_+ + x - 1)\right) - m^2\right]F(x) = 0, \tag{2.2.4}$$

this is the equation that will be worked with numerically. A solution to this differential equation is sought using a power series around $x = 0$, as follows

$$F = 1 + \sum_{i=1}^{n} a_i x^i + \mathcal{O}(x)^{n+1}. \tag{2.2.5}$$

The coefficients a_i are determined order by order. Using this expression, F and F' are fixed near $x = 0$ and then the integration is performed numerically. Note that the initial condition cannot be imposed at $x = 0$ or $x = 1$ since they are singular points of the differential equation to solve, therefore it is convenient to consider $x = x_{reg} \sim 1/10$. Computing up to the first derivative of (2.2.5), which is evaluated at x_{reg} to give the initial conditions. The next step is to integrate over the radial coordinate and plot the value of the solution at $x = 1$ as a function of the frequency. The solution is required to vanish at $x = 1$, values which correspond to zero on the plot. For this problem, the frequencies are complex numbers. Recall that we discussed the explicit form of the spectrum earlier, this system is intended to be used only as a test for the numerical routine. By setting $Re(\omega) = 1$, the horizontal axis is left for the imaginary part.

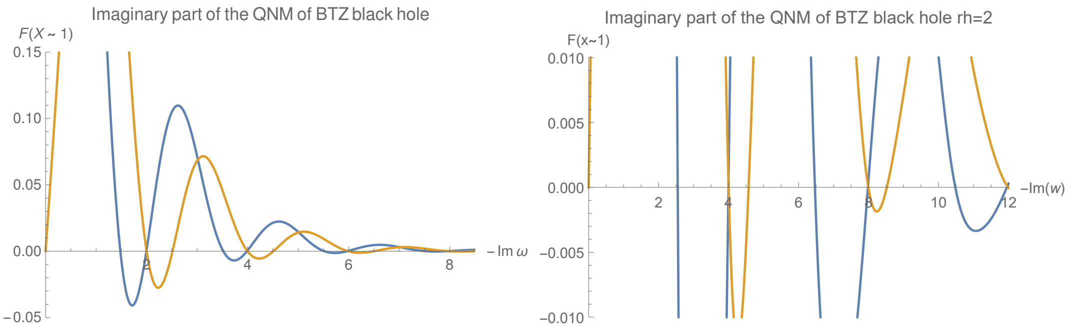

Figure 2.2.1: Imaginary part of the quasi-normal modes of the static BTZ black hole. Here $Re(\omega) = 1$, $r_+ = 1$ (left) and $r_+ = 2$ (right). The intersection between the yellow and blue curves corresponds to the imaginary part of the frequencies which solve the boundary value problem.

We have obtained a good accuracy if we compare with the analytical results given by the expression

$$\omega = m - 2(q+1)r_+ i. \tag{2.2.6}$$

Note that in the Figure 2.2.1 the results are aproximate for the imaginary part of the frequency.

Chapter 3

Schwarzschild AdS black hole

It is interesting to explore quasi-normal modes in a geometry where they can only be obtained numerically, such as in the Schwarzschild-AdS black hole. We will present results that can be compared with those obtained in the paper [4], where a different numerical method was employed.

The metric that characterizes this four-dimensional geometry is as follows

$$ds^2 = -f(r)dt^2 + \frac{dr^2}{f(r)} + r^2 d\theta^2 + r^2 \sin^2(\theta) d\phi^2, \tag{3.0.1}$$

that has the domain in $-\infty < t < +\infty,\ r_+ < r < +\infty,\ 0 \leq \theta < \pi,\ 0 \leq \phi < 2\pi$, identified. In addition, the function $f(r)$ is defined

$$f(r) = \frac{r^2}{l^2} + 1 - \frac{r_+}{r}\left(\frac{r_+^2}{l^2} + 1\right). \tag{3.0.2}$$

This spacetime is also a solution of Einstein equation with a negative cosmological constant, namely, it solves

$$G_{\mu\nu} + \Lambda g_{\mu\nu} = 0 \tag{3.0.3}$$

with $\Lambda = -\frac{3}{l^2}$. Correspond to a black hole with horizon located at $r = r_+$ and it is asymptotically AdS. Working with the Klein Gordon equation for a massless scalar field

$$\frac{1}{\sqrt{-g}}\partial_\mu\left(\sqrt{-g}g^{\mu\nu}\partial_\nu\Phi\right)=0, \tag{3.0.4}$$

we introduce the following scalar field[1]

$$\Phi(t,r,\theta,\phi)=\frac{\psi(r)}{r}\mathrm{Y}(\theta,\phi)e^{-i\omega t}, \tag{3.0.5}$$

where $\mathrm{Y}(\theta,\phi)$ are spherical harmonics. Then, a second-order differential equation with derivatives for $Y(\theta,\phi)$ and $\psi(r)$ according to their dependencies, is obtained. Spherical harmonics satisfies the equation

$$l(l+1)Y(\theta,\phi)+\frac{1}{\sin\theta}\frac{\partial}{\partial\theta}\left(\sin\theta\frac{\partial Y(\theta,\phi)}{\partial\theta}\right)+\frac{1}{\sin^2\theta}\frac{\partial^2 Y(\theta,\phi)}{\partial\phi^2}=0, \tag{3.0.6}$$

which allows us to write the differential equation with the angular part separated from the radial one.

Now, we focusses the radial dependence, performing the change of variable

$$r=\frac{r_+}{1-x}, \tag{3.0.7}$$

where $0<x<1$. This results in a differential equation that depends solely on x. Analyzing the obtained result and searching for solutions near the horizon ($x=0$) to first order using Frobenius method, leads to the solution

$$\Psi(r(x))\sim x^{\pm\frac{l^2\omega r_+}{l^2+3r_+^2}i}(1+\mathcal{O}(x)). \tag{3.0.8}$$

The wave must be ingoing at $r=r_+$, which correspond to the event horizon and is represented by the negative sign in the exponent of x in (3.0.8). We then propose the following form for the scalar field

$$\Psi(x)=x^{-\frac{l^2\omega r_+}{l^2+3r_+^2}i}F(x). \tag{3.0.9}$$

This formulation for the scalar field will be used in the differential equation

[1]As before, one could integrate in ω and add over spherical harmonics, but since the equation is linear, modes decouple.

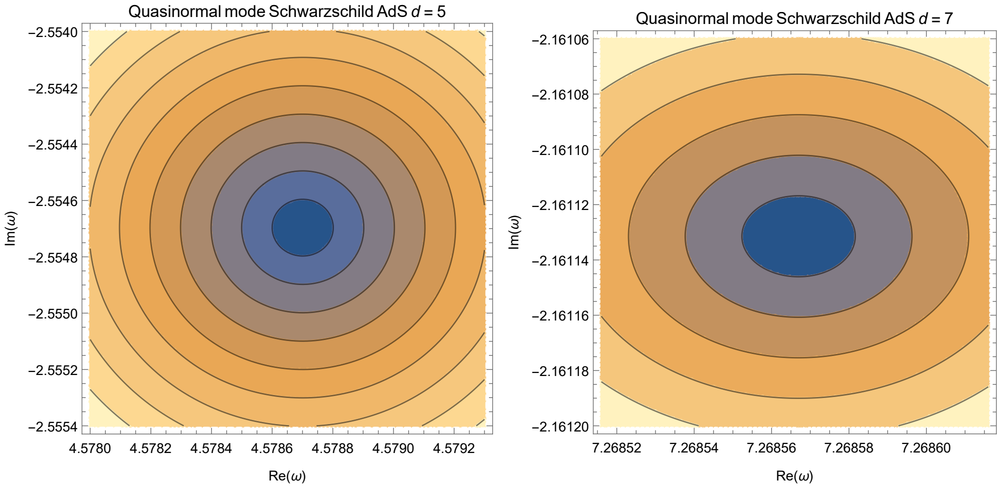

Figure 3.0.1: Quasi-normal modes of the Schwarzschild black hole in AdS. On the left panel is the fundamental mode in five dimensions, while on the right panel is the fundamental mode in seven dimensions.

obtained after the change of variable, resulting in a differential equation with derivatives of the function $F(x)$, that can be solved by seeking solutions in the form of power series,

$$F(x) = 1 + \sum_{i=1}^{N} (\ a_i x^i\ ) + \mathcal{O}(x)^{N+1}. \tag{3.0.10}$$

Considering the series (3.0.10) as the function $F(x)$ in the differential equation obtained after proposing (3.0.9), allows us to extract coefficients according to the power of x.

Finally, it is possible to plot the value of $|F(x)|$ at infinity ($x \sim 1$) as a function of $\omega \in \mathbb{C}$. The same numerical method explained in the final part of Section 2 has been used. Note that in Figure 3.0.1 the value of one of the quasi-normal modes appear in five and seven dimensions respectively. These results agree with those in table 1 of reference [4].

Chapter 4

Rotating black holes and static solitons in Einstein-Gauss-Bonnet at the Chern-Simons point

The quasi-normal modes of rotating black holes and solitons have not been explored so far in the Einstein-Gauss-Bonnet theory at the Chern-Simons point. In particular, we will focus on the following action defined in five dimensions

$$I = \int d^5x\sqrt{-g}\left(R - 2\Lambda + \alpha\left(R^2 - 4R_{ab}R^{ab} + R_{abcd}R^{abcd}\right)\right). \tag{4.0.1}$$

The Chern-Simons point correspond to choose the following special line:

$$\alpha = \frac{l^2}{4} \quad \text{and} \quad \Lambda = -\frac{3}{l^2}, \tag{4.0.2}$$

where α is a coupling parameter, Λ the cosmological constant and l is the AdS radius of the single maximally symmetric solution.

In this theory the field equations are

$$G_{ab} + g_{ab}\Lambda + \alpha\left(2RR_{ab} - 4R_{adbc}R^{dc} + 2R_{adce}R_b{}^{dce} - 4R_{ad}R^d{}_a - \frac{1}{2}g_{ab}L_{GB}\right) = 0, \tag{4.0.3}$$

where the Einstein tensor is

$$G_{ab} = R_{ab} - \frac{1}{2} g_{ab} R, \tag{4.0.4}$$

and the Gauss-Bonnet density reads

$$L_{GB} = R_{jklm} R^{jklm} - 4 R_{jk} R^{jk} + R^2. \tag{4.0.5}$$

The static BTZ-like black hole [2] is a solution to this theory, which is given by

$$ds^2 = -f(r) dt^2 + \frac{dr^2}{f(r)} + r^2 d\Omega_3^2, \tag{4.0.6}$$

with

$$f(r) = \frac{r^2}{l^2} - M, \tag{4.0.7}$$

and the domain $-\infty < t < +\infty$ and $r_+ < r < +\infty$, and $d\Omega_3$ stands for the line element of the three sphere.

The result of quasi-normal modes of scalars on this geometry exist in the literature [6].

An interesting aspect to review is the temperature of the black hole, which can be determined through

$$T = \frac{\kappa}{2\pi}, \tag{4.0.8}$$

where κ is the surface gravity that in this case reads

$$\kappa = \frac{1}{2} |f'(r)|_{r=r_+}, \tag{4.0.9}$$

resulting in

$$T = \frac{r_+}{2\pi l^2}. \tag{4.0.10}$$

On the other hand, this metric is static and contains no cross terms, so its angular momentum vanishes.

4.1 Two rotating black holes and two static solitons

A recent rotating solution to this theory can be found in the literature [5], characterized by the mass M, angular momentum j and a hair of gravitational origin b

$$ds^2 = l^2 \cosh^2(\rho)\left[-N^2dt^2 + \frac{dr^2}{N^2} + r^2(d\psi + N^\psi dt)^2\right] + l^2 d\rho^2 + l^2 C^2(\rho)dx^2, \tag{4.1.1}$$

where the lapse function and the shift are

$$N^2 = r^2 - M - \frac{b}{r} + \frac{j^2}{4r^2} \quad \text{and} \quad N^\psi = -\frac{j}{2r^2}. \tag{4.1.2}$$

The range of the coordinates are $-\infty < t < \infty$, $-\infty < \rho < \infty$, $-\infty < x < +\infty$, $r_+ \leq r < \infty$, and $0 \leq \psi < 2\pi$, identified. Hereafter we set the value $\rho_0 = 0$, since in this way we can integrate the equation for the ρ dependence of a scalar, in closed manner.

Note that the last term of (4.1.1) corresponds to a function of ρ. In particular we will work with two families of solutions, the first of them is a solution that is already known [5]

$$ds_I^2 = l^2 \cosh^2(\rho)\left[-N^2dt^2 + \frac{dr^2}{N^2} + r^2(d\psi + N^\psi dt)^2\right] + l^2 d\rho^2 + l^2 \cosh^2(\rho)dx^2, \tag{4.1.3}$$

and we classify it as Family I.

Now we introduce a new solution,

$$ds_{II}^2 = l^2 \cosh^2(\rho)\left[-N^2dt^2 + \frac{dr^2}{N^2} + r^2(d\psi + N^\psi dt)^2\right] + l^2 d\rho^2 + l^2 e^{2\rho}dx^2, \tag{4.1.4}$$

that correspond to Family II.

In addition, from these geometries it is possible to construct static solitons. First of all consider the static metric, which involves canceling the angular momentum from (4.1.1),

$$ds^2_{I,II} = l^2 \cosh^2(\rho) \left[-N^2 dt^2 + \frac{dr^2}{N^2} + r^2 d\psi^2 \right] + l^2 d\rho^2 + l^2 C^2(\rho) dx^2. \tag{4.1.5}$$

Then doing the double-Wick rotation ($t \to iy,\ \psi \to it$), which affects only the term within the bracket, we arrive to the spacetimes

$$ds^2_{I,II} = l^2 \cosh^2(\rho) \left[-r^2 dt^2 + \frac{dr^2}{N^2} + N^2 dy^2 \right] + l^2 d\rho^2 + l^2 C^2(\rho) dx^2. \tag{4.1.6}$$

This changes the domain of the radial coordinate, it is redefined to be $r_0 < r < +\infty$ where r_0 is the largest root of

$$N^2(r_0) = r_0^2 - M - \frac{b}{r_0} = 0, \tag{4.1.7}$$

representing the size of the soliton where we have set $l = 1$. The mass can be written as a function of the parameter r_0

$$M(r_0) = r_0^2 - \frac{b}{r_0}, \tag{4.1.8}$$

which leads to

$$N^2(r) = r^2 - \left(r_0^2 - \frac{b}{r_0} \right) - \frac{b}{r}. \tag{4.1.9}$$

In this way, the three-dimensional bracket metric (4.1.6) approaches to

$$ds^2 \simeq -r^2 dt^2 + \frac{dr^2}{\left(r^2 - r_0^2 - \frac{b}{r_0} - \frac{b}{r} \right)} + \left(r^2 - r_0^2 - \frac{b}{r_0} - \frac{b}{r} \right) dy^2. \tag{4.1.10}$$

It can be noted that r_0 is a singular point in the metric, but it is interesting to study the behavior near this value. To work on this problem, a Taylor series expansion around the soliton origin is performed. Considering only leading terms,

$$N^2(r) = N^{2\prime}(r)|_{r_0} (r - r_0). \tag{4.1.11}$$

In addition, a variable change can be made that satisfies

$$d\rho = \frac{dr^2}{\sqrt{N^{2\prime}(r)|_{r_0}(r-r_0)}}, \tag{4.1.12}$$

which implies

$$\rho = 2\sqrt{\frac{(r-r_0)}{N^{2\prime}(r)|_{r_0}}}. \tag{4.1.13}$$

This allows the metric in (4.1.10) to be rewritten as follows

$$ds^2 \simeq -r_0^2 dt^2 + d\rho^2 + \frac{(N^{2\prime}(r)|_{r_0})^2}{4}\rho^2 dy^2. \tag{4.1.14}$$

Observe that the final two terms locally describe flat space in polar coordinates; hence, the metric can be simplified by considering

$$\psi = \frac{N^{2\prime}(r)|_{r_0}}{2} y, \tag{4.1.15}$$

such that the coordinate ψ will be periodic of the domain $0 \leq \psi \leq 2\pi$ to avoid conical singularities, and therefore

$$2\pi = \frac{N^{2\prime}(r)|_{r_0}}{2}\Delta_y. \tag{4.1.16}$$

Solving for Δ_y,

$$\Delta_y = \frac{4\pi r_0^2}{2r_0^3 + b}, \tag{4.1.17}$$

which represents the period of the coordinate y.

Therefore, there are two families of solution and each one contains a rotating black hole and a static soliton solutions.

4.2 Scalar probes

We will explore the propagation of scalar probes in the geometries (4.1.3), (4.1.4) and (4.1.6). Each of them is contained in the following family of metrics

$$d\tilde{s}^2 = A^2(\rho)g_{\mu\nu}dx^\mu dx^\nu + l^2 d\rho^2 + C^2(\rho)dx^2, \tag{4.2.1}$$

note that the first term contains the three-dimensional spacetime, so it is possible to continue the analysis in a general way considering the mentioned geometries in five dimensions.

Let us now consider the massless Klein Gordon equation

$$\frac{1}{\sqrt{-g}}\partial_\mu\left(\sqrt{-g}g^{\mu\nu}\partial_\nu\Phi\right) = 0, \tag{4.2.2}$$

on the geometries (4.2.1), and the ansatz for the scalar field

$$\Phi(x^A) = \psi(x^\mu)Y(\rho)e^{ikx}, \tag{4.2.3}$$

which leads to two differential equations, after introducing the separation constant m^2_{eff}, one of them depending on x^μ and the other on ρ,

$$\partial_\rho(A^3C\partial_\rho Y(\rho)) + A^3Cl^2\left(\frac{m^2_{\text{eff}}}{A^2} - \frac{k^2}{C^2}\right) = 0, \tag{4.2.4}$$

$$\Box_3\psi(x^\mu) - m^2_{\text{eff}}\psi(x^\mu) = 0. \tag{4.2.5}$$

Note that the name of the separation constant is due to the form of the second differential equation, since it is interpreted as the mass, and $\Box_3$ is the wave operator according to the three-dimensional metric in (4.2.1).

We will start by solving the differential equation for ρ (4.2.4), first to the Family I and then for Family II.

In Family I the functions are defined as $A(\rho) = l\cosh(\rho) = C(\rho)$, thus we obtain

$$\cosh^2(\rho)\frac{d^2Y(\rho)}{d\rho^2} - (k^2 - m^2_{\text{eff}})Y(\rho) = 0. \tag{4.2.6}$$

Performing the change of coordinates $z = \tanh(\rho)$

$$(z^2-1)\frac{d^2Y(z)}{dz^2} + 2z\frac{dY(z)}{dz} + (k^2 - m_{\text{eff}}^2)Y(z) = 0, \tag{4.2.7}$$

mapping range $-\infty < \rho < +\infty$ to $-1 < z < 1$. Solve the differential equation leads to a solution in term of Legendre functions of the first and second kind

$$Y(z) = C_1\ (z^2-1)P_\nu^\mu + C_2\ (z^2-1)Q_\nu^\mu, \tag{4.2.8}$$

where $\mu = 2$ and $\nu = \frac{\sqrt{4(m_{\text{eff}}-k^2)+9}-1}{2}$, C_1 and C_2 are integration constants.

Writing the solution in terms of Hypergeometric functions leads to

$$\begin{aligned} Y(z) = \bar{C}_1(1-z^2)^2\ {}_2F_1\left(-\bar{a}+\frac{5}{2}, \bar{a}+\frac{5}{2}, 3, \frac{1-z}{2}\right) \\ + C_2\frac{(z^2-1)^2}{z^{\bar{a}+\frac{5}{2}}}\frac{\Gamma\left(\bar{a}+\frac{5}{2}\right)}{\Gamma(\bar{a}+1)}\ {}_2F_1\left(\frac{2\bar{a}+7}{4}, \frac{2\bar{a}+5}{4}, \bar{a}+1, z^{-2}\right), \end{aligned} \tag{4.2.9}$$

with

$$\bar{a} = \frac{\sqrt{4(m_{\text{eff}}^2-k^2)+9}}{2}. \tag{4.2.10}$$

Notice that in the limit $z \to 1$, the first term goes to a constant since the argument of Hypergeometric function cancels out, while the second term does not become a constant, since the argument of the Hypergeometric function becomes one. The Kummer identities [3] allow us to rewrite the second Hypergeometric function in order to cancel its argument,

$$\begin{aligned} {}_2F_1\left(a,b,c,z^{-2}\right) = & \frac{\Gamma(c)\Gamma(-a-b+c)}{\Gamma(-a+c)\Gamma(-b+c)}\ {}_2F_1\left(a,b,a+b-c+1,1-z^{-2}\right) \\ & +\ {}_2F_1\left(-a+c,-b+c,-a-b+c+1,1-z^{-2}\right) \\ & \times (1-z^{-2})^{-a-b+c}\frac{\Gamma(c)\Gamma(a+b-c)}{\Gamma(a)\Gamma(b)}, \end{aligned} \tag{4.2.11}$$

where

$$a = \frac{2\bar{a}+7}{4}, \tag{4.2.12}$$

$$b = \frac{2\bar{a}+5}{4}, \tag{4.2.13}$$

$$c = \bar{a}+1. \tag{4.2.14}$$

Therefore the solution for $Y(z)$ behaves well at the boundary $z \to 1$. However, when rewriting the Hypergeometric function, a new term z arises, whose powers grow very fast with those in (4.2.9). Hence, setting $C_2 = 0$ allows removing such divergence, leaving

$$Y(z) = \bar{C}_1(1-z^2)^2 \; {}_2F_1\left(-\bar{a}+\frac{5}{2}, \bar{a}+\frac{5}{2}, 3, \frac{1-z}{2}\right). \tag{4.2.15}$$

The other boundary is at the value $z \to -1$. For this case it is possible see that the argument of the Hypergeometric function is not zero. Consequently, we follow the same procedure as above using the Kummer identities (4.2.11).

When rewriting, a term arises with Gamma functions that prevents the solution from being constant in this limit

$$Y(z \to 1) \approx C_1 \frac{\Gamma(\tilde{c})\Gamma(\tilde{a}+\tilde{b}-\tilde{c})}{\Gamma(\tilde{a})\Gamma(\tilde{b})}, \tag{4.2.16}$$

where

$$\tilde{a} = -\bar{a}+\frac{5}{2}, \tag{4.2.17}$$

$$\tilde{b} = \bar{a}+\frac{5}{2}, \tag{4.2.18}$$

$$\tilde{c} = 3. \tag{4.2.19}$$

As mentioned above, Gamma functions are defined only if their argument is not a negative integer or zero, if takes that value it diverges. Therefore, this can be used to define the value of the constant in the argument of one of the Gamma functions in the denominator and thus cancel it out, making $Y(z \to -1)$ constant. Therefore, this procedure can be performed with the argument $\tilde{a}$ or $\tilde{b}$. We will continue working with the argument $\tilde{b}$

$$\frac{\sqrt{4(m_{\text{eff}}^2 - k^2) + 9}}{2} + \frac{5}{2} = -p, \tag{4.2.20}$$

with $p = 0, 1, 2, ...$ leaving the solution

$$Y_I(\rho(z)) = C_1(1 - z^2)^2 \,{}_2F_1\left(-p, 5 + p, 3, \frac{1 - z}{2}\right), \tag{4.2.21}$$

which behaves well in both limits.

Solving the differential equation for the Family I (4.2.6) allowed us to know the form of the separation constant

$$m_{\text{eff}}^2 = m_I^2 = k^2 + (p + 1)(p + 4). \tag{4.2.22}$$

We will now study (4.2.4) for Family II, where the functions are defined as $A(\rho) = l \cosh(\rho)$ and $C(\rho) = le^{\rho}$, which leads to

$$\begin{aligned} \cosh^2\rho \, \frac{d^2Y(\rho)}{d\rho^2} &+ \cosh\rho \,(\cosh\rho + 3\sinh\rho)\, \frac{dY(\rho)}{d\rho} \\ &- \left(k^2 e^{-2\rho} \cosh^2\rho - m_{\text{eff}}^2\right) Y(\rho) = 0. \end{aligned} \tag{4.2.23}$$

Solving this equation provides a solution in terms of confluent Heun functions,

$$\begin{aligned} Y(\rho) = \;& K_1(e^{-2\rho} + 1)^{\sqrt{m_{\text{eff}}^2+1}} \text{HC}\left(0, 2\sqrt{m_{\text{eff}}^2 + 1}, 2, -k^2/4, m_{\text{eff}}^2 + 2, e^{-2\rho} + 1\right) \\ +\;& K_2(e^{-2\rho} + 1)^{-\sqrt{m_{\text{eff}}^2+1}} \text{HC}\left(0, -2\sqrt{m_{\text{eff}}^2 + 1}, 2, -k^2/4, m_{\text{eff}}^2 + 2, e^{-2\rho} + 1\right). \end{aligned} \tag{4.2.24}$$

When k vanishes it is possible to rewrite the solution using Hypergeometric functions, which we use after performing the change of coordinates $z = \tanh(\rho)$, leading to

$$\begin{aligned} Y(\rho) = \;& K_1(z - 1)^{\bar{b}} \,{}_2F_1\left(\bar{b}, \bar{b} + 2, 2\bar{b} + 1, -\frac{2}{z - 1}\right) \\ +\;& K_2(z - 1)^{-\bar{b}} \left(\frac{z + 1}{z - 1}\right)^2 \,{}_2F_1\left(-\bar{b}, -\bar{b} + 2, -2\bar{b} + 1, -\frac{2}{z - 1}\right), \end{aligned} \tag{4.2.25}$$

where $\bar{b} = \sqrt{m_{\text{eff}}^2 + 1}$.

In the same way as before, using the Kummer identities it is possible to rewrite the hypergeometric functions so that they are regular in the limits, that is when $z \to 1$ and $z \to -1$, obtaining as a result

$$Y_{II}(\rho(z)) = A(1-z)^2 \, {}_2F_1\left(-p-1, p+3, 3, \frac{1-z}{2}\right), \tag{4.2.26}$$

with $p = 0, 1, 2, \ldots$.

Imposing regularity of the solution on the boundaries of z, it is necessary to work again with the argument of the Gamma function. Thus, the separation constant for this case has the form

$$m_{\text{eff}}^2 = m_{II}^2 = (p+1)(p+3). \tag{4.2.27}$$

So far we have solved the equation (4.2.4) for both geometries and the information it has provided us is the values of the separation constant, (4.2.22) and (4.2.27). These results are valid for both the soliton and the black hole of Family I and II, as appropriate.

4.3 Scalar probes on solitons

Solving the three-dimensional Klein-Gordon equation (4.2.5), will allow us to obtain the normal frequencies in the static soliton geometries

$$ds_{3,sol}^2 = -r^2 dt^2 + \frac{dr^2}{\left(r^2 - M - \frac{b}{r}\right)} + \left(r^2 - M - \frac{b}{r}\right) dy^2, \tag{4.3.1}$$

with $-\infty < t < +\infty,\ r_0 \leq r < +\infty$, and $0 \leq y \leq \Delta_y$.

Assuming the separation for the scalar probe

$$\psi(x^\mu) = e^{-i\omega t + i\frac{2\pi n}{\Delta_y} y} R(r), \tag{4.3.2}$$

with $n \in \mathbb{N}$.

Thus, the Klein-Gordon equation leads to

$$N^2\,\frac{d^2R(r)}{dr^2}+\left(3r-\frac{M}{r}\right)\frac{dR(r)}{dr}+\left(\frac{\omega^2}{r^2}-m_{\text{eff}}^2-\frac{4\pi^2n^2}{\Delta_y^2}\frac{r^2}{N^2}\right)R(r)=0, \quad (4.3.3)$$

where $N(r)$ is defined in (4.1.2).

This second order differential equation admits two asymptotic behaviors. In the limit as r tends to r_0,

$$R(r)\sim C_1(r-r_0)^{\frac{n}{2}}(1+\mathcal{O}(r-r_0))+C_2(r-r_0)^{-\frac{n}{2}}(1+\mathcal{O}(r-r_0)), \qquad (4.3.4)$$

and on the limit towards infinity

$$R(r)\sim\frac{D_1}{r^{\Delta_+}}(1+\mathcal{O}(r^{-1}))+\frac{D_2}{r^{\Delta_-}}(1+\mathcal{O}(r^{-1})), \qquad (4.3.5)$$

with

$$\Delta_\pm=1\pm\sqrt{1+m_{\text{eff}}^2}. \qquad (4.3.6)$$

Next we analyze each behavior. For equation (4.3.4) we choose the term with positive exponent, which will vanish as r approaches r_0. On the other hand, the term with negative exponent will diverge in this limit. Therefore, we impose regularity by setting $C_2=0$. For equation (4.3.5), the exponential of r depends on the effective mass parameter, where m_{eff}^2 is strictly positive, as shown by (4.2.22) and (4.2.27). Therefore, to ensure that the solution does not diverge since in (4.3.6) the subtraction can be negative, we impose Dirichlet boundary conditions which involve setting $D_2=0$ when $r\to\infty$.

After performing this analysis, the calculation to solve the radial equation is purely numerical. We solve it by interpolating and clearing the normal modes ω in a similar way to the numerical method used in section 2.2. The frequencies depend on the parameters m_{eff}, n, q that label the modes and on the parameterization of the soliton b/r_0^3 , that is, $\omega=\omega\left(\frac{b}{r_0^3}, m_{\text{eff}}, n, q\right)$.

In particular, the frequencies can be analyzed using two forms of parameterization, both of which are dimensionless, which are $(b/r_0^3, \omega/r_0)$ and $(r_0/b^{1/3}, \omega/b^{1/3})$. This allows us to study how the normal frequencies behave as a function of the gravitational hair b and as the soliton parameterization varies.

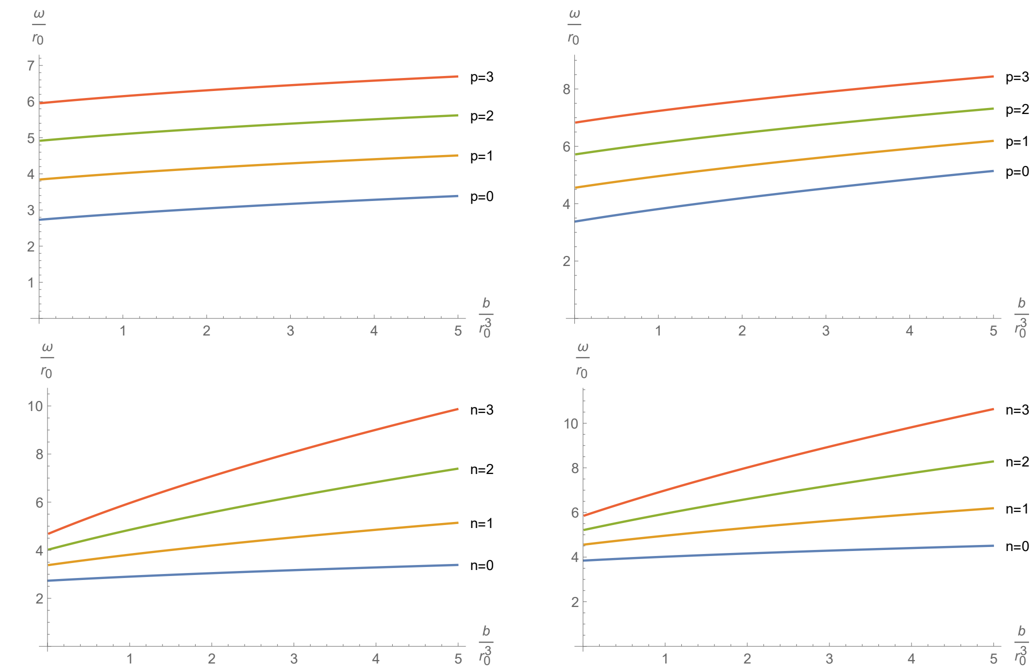

Figure 4.3.1: Normal modes for the scalar field over Family I solitons analyzed by varying the parameter b. Considering $k = 0$ in 4.2.22 the curves correspond to different effective masses $m_{\text{eff}}(p)$ with $n = 0$ in the upper left and $n = 1$ for the upper right. In the lower-left panel the analysis correspond to the adjustment $m_{\text{eff}}(p = 0)$ where the curves represent different values of the angular momentum n of the scalar field, while the lower-right panel considers the value $m_{\text{eff}}(p = 1)$.

First of all, it is necessary to note that for small values of r_0 the solitons will have a larger size and that by increasing the value of r_0 they will become smaller, in any regularized version of their spatial value. In the first case, Figure 4.3.1, we analyze the frequencies as a function of the gravitational hair b starting from zero, a study that is shown for Family I to lead to the same qualitative behavior as for Family II. As the latter increases, the frequencies also become higher, acquiring a monotonic behavior. For the case where the analysis is performed with respect to the size of the soliton, Figure 4.3.2 , it can be observed that an interesting result occurs when the value of r_0 is very small. As the soliton becomes smaller, that is for increasing values of r_0, the fundamental frequencies should increase. On the other hand, as r_0 decreases, the frequency value should also decrease, however, we observe the opposite. This shows that there is a critical value for r_0, which we will refer to as r_c. It is clearly seen in the Figure 4.3.2 that for $r_0 < r_c$ the slope of the curve $\omega = \omega(r_0)$ is negative and when $r_0 > r_c$ it changes sign, increasing the frequency. The point at which the slope changes varies according to the mode considered.

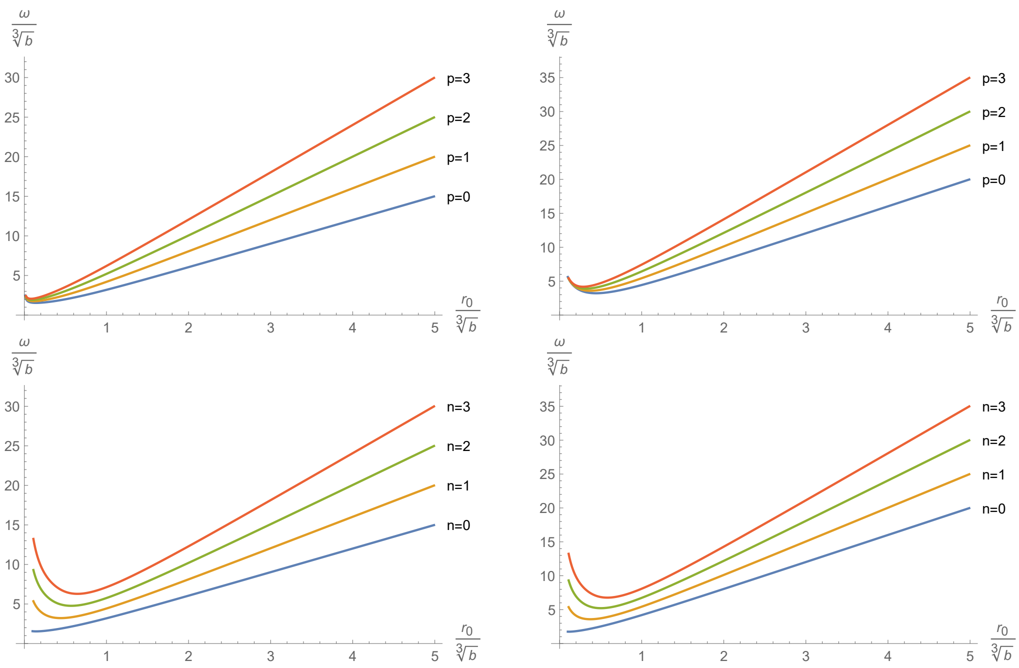

Figure 4.3.2: Frequencies for solitons of Family I are presented as a function of the soliton size parametrization $r_0/\sqrt[3]{b}$. Angular momentum n of the field is fixed zero in upper-right plot, which shows curves for different values of mass $m_{\text{eff}}(p)$ with $k=0$, while in the upper-left, n is set to one. The curves at the bottom represent different values for n with a fixed effective mass, $m_{\text{eff}}(p=0)$ on the left and $m_{\text{eff}}(p=1)$ on the right.

4.4 Scalar probes on black holes

Previously, the five-dimensional problem was simplified by introducing a separation constant, resulting in the effective Klein-Gordon equation, which we have already solved for the geometry of the static soliton. Next, we will explore equation (4.2.5) for the geometry of a three-dimensional rotating black hole described by the following metric

$$ds^2_{3,BH} = -N^2 dt^2 + \frac{dr^2}{N^2} + r^2 \left(d\phi - \frac{j}{2r^2} dt \right)^2, \tag{4.4.1}$$

where $N(r)$ is given as before by equation (4.1.2). Additionally, for simplicity, the mass parameter of the black hole can be expressed in terms of its horizon location r_+, as follows

$$M = \frac{4r_+^4 - 4br_+ + j^2}{4r_+^2}. \tag{4.4.2}$$

It is possible to calculate the temperature of a black hole, denoted as T, using

$$T = \frac{\kappa}{2\pi}, \tag{4.4.3}$$

where the square of the surface gravity reads

$$\kappa^2 = -\frac{1}{2}\, \xi_{\mu;\nu}\xi^{\mu;\nu}\big|_{r=r_+}. \tag{4.4.4}$$

In our case:

$$T = \frac{1}{4\pi}\left|-\frac{dg_{tt}}{dr}\right|_{r=r_+} \tag{4.4.5}$$

$$= \frac{1}{4\pi}\frac{4r_+^4 + 2br_+ - j^2}{2r_+^3}. \tag{4.4.6}$$

Moreover, the angular velocity of the horizon can be determined using the following straightforward expression,

$$\Omega_h = -\left.\frac{g_{t\phi}}{g_{\phi\phi}}\right|_{r=r_+} \tag{4.4.7}$$

$$= \frac{j}{2r_+^2}. \tag{4.4.8}$$

Furthermore, assuming the separation of the term defined above in equation (4.2.3), given by

$$\psi(x^\mu) = e^{-i\omega t + in\phi}R(r), \tag{4.4.9}$$

with $n = 0, \pm1, \pm2, ...$, leads to the equation

$$N^2(r)\frac{d^2R}{dr^2} + \left(3r - \frac{j^2}{4r^2} - \frac{M}{r}\right)\frac{dR}{dr} - \left(m_{\text{eff}}^2 + \frac{n^2}{r^2} - \frac{(jn - 2\omega r^2)^2}{4r^4N^2(r)}\right)R = 0. \tag{4.4.10}$$

To solve this equation, we will begin with the simplest case that can be solved analytically, namely, by setting $b = 0$. This reduces the problem to the geometry of the rotating BTZ black hole, as can be seen in the equation (4.4.1), which we will discuss next.

It is feasible to ascertain the form of the function $R(r)$ utilizing the Frobenius method. We postulate behavior near the horizon $r = r_+$ when $b = 0$ conforms to a solution of the form [3]

$$\begin{aligned} R(r) = B_1(r - r_+)^{-\frac{(2r_+^2\omega - nj)r_+}{4r_+^4 - j^2}i}(1 + \mathcal{O}(r - r_+)) \\ + B_2(r - r_+)^{\frac{(2r_+^2\omega - nj)r_+}{4r_+^4 - j^2}i}(1 + \mathcal{O}(r - r_+)), \end{aligned} \tag{4.4.11}$$

where B_1 and B_2 are constants.

We impose ingoing boundary conditions at that point by selecting the branch with the negative sign for the exponent of r_+. Therefore,

$$R(r) = (r - r_+)^{-\frac{(2r_+^2\omega - nj)r_+}{4r_+^4 - j^2}i}F(r), \tag{4.4.12}$$

where the function $F(r)$ must satisfy $(1 + \mathcal{O}(r - r_+))$. Substituting this result into equation (4.4.10), we obtain a differential equation for the function $F(r)$, which upon solving reveals the form

$$F(r) = B_1(4r^2r_+^2 - j^2)^{\frac{r_+(-j\omega + 2nr_+^2)}{4r_+^4 - j^2}i}(r + r_+)^{-\frac{r_+(2r_+^2\omega - nj)}{4r_+^4 - j^2}i}\,{}_2F_1\left(a, b, c, -\frac{z}{1 - z}\right), \tag{4.4.13}$$

where

$$z(r) = \frac{(r^2 - r_+^2)}{r^2 - j^2/4r_+^2}, \tag{4.4.14}$$

and

$$a = \frac{\sqrt{k^2 - m_{\text{eff}}^2 + 1} + 1}{2} - \frac{(\omega - n)r_+}{2r_+^2 - j}i, \tag{4.4.15}$$

$$b = \frac{\sqrt{k^2 - m_{\text{eff}}^2 + 1} + 1}{2} - \frac{(\omega + n)r_+}{2r_+^2 + j}i, \tag{4.4.16}$$

$$c = 1 + \frac{2r_+(2r_+^2\omega - jn)}{4r_+^4 - j^2}i. \tag{4.4.17}$$

When analyzing the behavior of equation (4.4.13) as $r \to +\infty$, it becomes necessary to rewrite the Hypergeometric function, ensuring the solution remains regular at the extremes. This is achieved by employing Kummer's identities, which allow us to work with an argument that approaches zero as r tends to infinity,

$$\begin{aligned} {}_2F_1(a,b,c,\tilde{z}(r)) = & \frac{\Gamma(c)\Gamma(c-a-b)}{\Gamma(c-a)\Gamma(c-b)}\ {}_2F_1(a,b,a+b+1-c,1-\tilde{z}(r)) \\ & + \ {}_2F_1(c-a,c-b,1+c-a-b,1-\tilde{z}(r)) \\ & \times \ \frac{\Gamma(c)\Gamma(a+b-c)}{\Gamma(a)\Gamma(b)}(1-\tilde{z}(r))^{c-a-b}. \end{aligned} \tag{4.4.18}$$

Consequently, the argument of the Hypergeometric function is reformulated as

$$1-\tilde{z}(r) = \frac{4r_+^4 - j^2}{4r_+^2 r^2 - j^2}, \tag{4.4.19}$$

which cancels out when we consider the limit $r \to \infty$. Rewriting the Hypergeometric function of equation (4.4.13) as indicated in (4.4.18) we obtain two terms, one of negative power and one of positive power. We expect that when r tends to infinity the field will be constant, which occurs for the negative power, while the positive power it diverges. To impose this behavior, as before we can take advantage of a property of Gamma functions. It diverges when its argument is negative, in this way

$$\frac{1}{2}\left(\sqrt{1+m_{\text{eff}}^2}+1\right) - r_+\frac{\omega+n}{2r_+^2+j}i = -n_1, \tag{4.4.20}$$

$$\frac{1}{2}\left(\sqrt{1+m_{\text{eff}}^2}+1\right) - r_+\frac{\omega-n}{2r_+^2-j}i = -n_2, \tag{4.4.21}$$

where n_1 and n_2 are mode numbers that take the values $\{0, \pm1, \pm2, ...\}$. Recall that we previously introduced an integration constant denoted as m_{eff}^2. Finally, it is possible to quantize the frequencies by working with $b=0$. We obtain the frequencies using equations (4.4.20) and (4.4.21), which leads us to

$$\omega_{n_1}^{(b=0)} = -n - \frac{2r_+^2+j}{2r_+}\left(2n_1+1+\sqrt{1+m_{\text{eff}}^2}\right)i, \tag{4.4.22}$$

$$\omega_{n_2}^{(b=0)} = \quad n - \frac{2r_+^2-j}{2r_+}\left(2n_2+1+\sqrt{1+m_{\text{eff}}^2}\right)i. \tag{4.4.23}$$

Note that (4.4.22) is analogous to (4.4.23), exchanging $n \leftrightarrow -n$ and $j \leftrightarrow -j$. This analytical result with $b = 0$ is known in the literature [6]. Obtaining this result allows us to understand the behavior of the frequency as the value of b increases.

The analytical results indicate the presence of modes with both positive and negative signs for the angular momentum of the scalar field n. When considering $j \geq 0$ and selecting a value for the angular momentum of the scalar field n, there will be modes that rotate in the opposite direction relative to the black hole (4.4.22) (since n is negative), as well as modes that rotate in the same direction (4.4.23). Furthermore, we have different signs for the imaginary parts of the frequencies since the sign of j changes, with the co-rotating modes being those with the longest lifetime since the imaginary part is closer to zero and therefore they are less damped than the counter-rotating ones.

To explore the quasi-normal frequencies with $b \neq 0$ we start by working on the BTZ geometry previously used for the analytical calculation, but this time introducing a variation by considering the parameter b.

We commence by proposing a power series solution around $r = r_+$ for $R(r)$, without canceling the parameter b as done previously. Furthermore, we impose that at the horizon, solution is incoming, leading to the result

$$R(r) = (r - r_+)^{-\frac{(2r_+^2\omega - nj)r_+}{4r_+^4 + 2br_+ - j^2}i} F(r), \tag{4.4.24}$$

where, once again, the function $F(r)$ is defined by $(1 + \mathcal{O}(r - r_+))$.

Substituting the proposed result for the function $R(r)$ into the equation (4.4.10), we derive an extensive differential equation for $F(r)$, which must be solved numerically. Before using it, we perform the change of variable

$$r = \frac{r_+}{1 - z}, \tag{4.4.25}$$

thus, we transition from domain $r \in [r_+, \infty)$ to $z \in [0, 1)$.

Utilizing the resulting differential equation and proposing as a standard power series for $F(r(z))$ as a solution, we determine its coefficients order by order, and then use Runge-Kutta numerical integration routines. The real and imaginary parts of the frequency when $b = 0$ are used as initial values, all within the

Mathematica program.

In addition to that method, we employed the QNMSpectral package to cross-check the frequency results. Further information can be found in the article [7] authored by A. Jansen. The initial step required to utilize this package was to transition to Eddington-Finkelstein incoming coordinates, this is primarily due to the method being designed to solve first order algebraic equations on the frequencies.

Let us begin by employing the following transformation to the metric (4.4.1) in the form

$$dv = dt + \frac{dr}{N(r)^2}, \quad d\tilde{\phi} = d\phi + \frac{j}{2r^2 N(r)^2}dt, \tag{4.4.26}$$

which leads to rewriting in terms of the ingoing Eddington-Finkelstein coordinates as follows

$$ds^2 = -N(r)^2 dv^2 + 2dvdr + r^2\left(d\tilde{\phi} - \frac{j}{2r^2}dv\right)^2. \tag{4.4.27}$$

Then, we consider the following scalar field

$$\psi(v, r, \tilde{\psi}) = e^{-i\omega v} J(r) e^{in\tilde{\phi}}. \tag{4.4.28}$$

Employing metric (4.4.27), with ansatz (4.4.28) in the massive Klein-Gordon equation defined above (4.2.5), one obtains the differential equation

$$\begin{aligned} r(r-r_+)[(4r_+^2r^2 - j^2)(r+r_+) + 4brr_+]\frac{d^2J(r)}{dr^2} \\ -[(4rr_+^2(2r^2\omega - jn)i - 12r^4 + j^2) + (4r^2r_+(r_+^3 - b) + j^2)]\frac{dJ(r)}{dr} \\ -2r_+^2[2r^2\omega + jn - 2r(2n^2 + r^2m_{\text{eff}}^2)i]J(r) = 0, \end{aligned} \tag{4.4.29}$$

that we entered into the program in Mathematica which integrates the QNMSpectral package. The results are presented in a graph and a table that lists the harmonic frequencies along with their real and imaginary parts, as illustrated in Figure 4.4.1. We focus on the fundamental mode, thus we extract the first value from each table as the parameter b increases. These values are stored in a list, which we use to plot the frequencies.

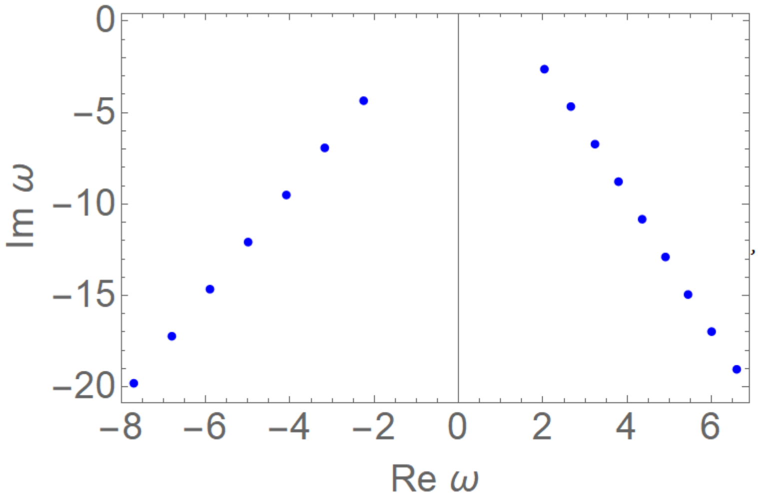

n	Re ω_n	Im ω_n
1	+ 2.034508019	−2.625906934
2	− 2.253514657	−4.349848671
3	+ 2.661293389	−4.668736256
4	+ 3.233913388	−6.724869120
5	− 3.176213483	−6.927991227
6	+ 3.791328308	−8.775512662
7	− 4.087205013	−9.504144843
8	+ 4.352673405	−10.82928356
9	− 4.994067374	−12.07881500
10	+ 4.905307119	−12.89417029
11	− 5.898969580	−14.65252416
12	+ 5.441411091	−14.94617251
13	+ 5.9996017	−16.9738298
14	− 6.80274208	−17.22559960
15	+ 6.596	−19.034
16	− 7.706	−19.798

Figure 4.4.1: Frequency results delivered using the QNMSpectral package, these correspond to a list of the modes for the entered values.

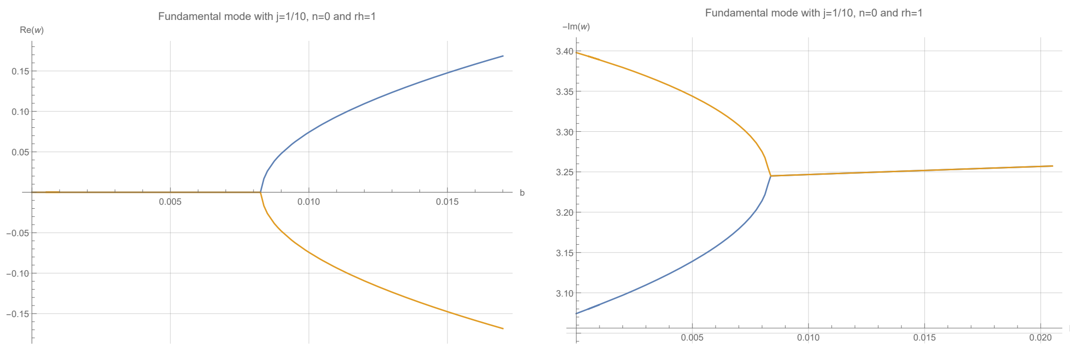

Figure 4.4.2: Behavior of the real (left) and imaginary (right) parts of the black hole fundamental mode frequencies as the parameter b increases. Fixed values are the angular momentum of the scalar field $n = 0$, the angular momentum of the black hole $j = 1/10$, the radius of the event horizon $r_+ = 1$ and the effective mass $m^2_{\text{eff}} = 4$.

Starting with the fundamental mode frequencies, using following values: $n = 0$ angular momentum along ϕ, black hole angular momentum $j = 1/10$, event horizon radius $r_+ = 1$, effective mass $m^2_{\text{eff}} = 4$, and increasing the hair parameter to $b \sim 0.02$. The resulting plot is presented in Figure 4.4.2.

Recall that we previously obtained two expressions for the frequency with value $b = 0$, (4.4.22) and (4.4.23). Note that result for both the real and imaginary parts, considering the smallest values of b that we can see in the Figure 4.4.2, is consistent with the analytical one, since the frequencies are purely imaginary for $n = 0$. However, we observe that there is a critical value of the hair parameter

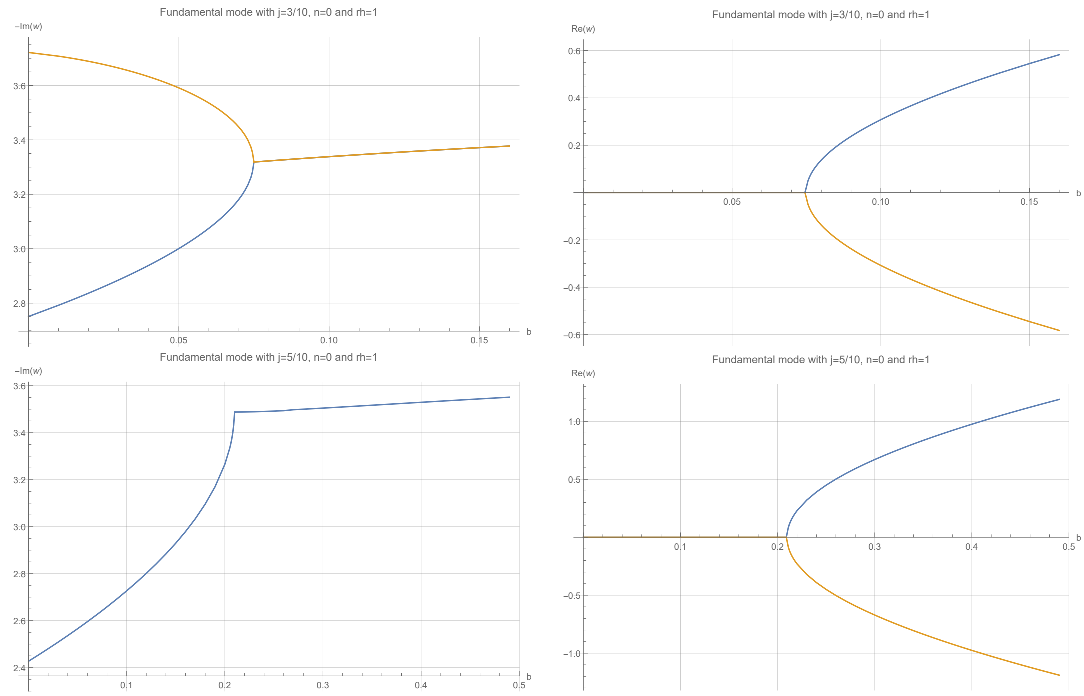

Figure 4.4.3: Behavior of the imaginary (left) and real (right) parts of the black hole fundamental mode frequencies for fixed values of angular momentum $j = 0.3$ (top) and $j = 0.5$ (bottom) as the parameter b increases. Furthermore, the angular momentum of the scalar field is $n = 0$, the radius of the event horizon $r_+ = 1$ and the effective mass $m^2_{\text{eff}} = 4$.

$b \sim 0.008$, where a bifurcation of the real part occurs, separating into two branches, one positive and one negative. Meanwhile, the imaginary part converges to a single value. Furthermore, the plot for $j = 0.3$ in the upper area of Figure 4.4.3 has a similar behavior for $j = 0.1$. However, for $j = 0.5$ it has been graphed only for the imaginary part with the highest value, since the other harmonics begin to cross with the fundamental mode, which does not allow to follow with precision the value for the branch with the highest damping. This behavior becomes more important as the value of the angular momentum of the black hole increases.

Another interesting analysis to review is how the frequency behaves for the fundamental mode when considering the angular momentum for the non-zero n scalar field . For this, we work with $n = 1$, set the value of b for each curve, and vary the angular momentum of the black hole j, keeping the other values constant, that is, $r_+ = 1$ and $m^2_{\text{eff}} = 4$. The results can be seen in the Figure 4.4.4, where the behavior is different. The values are indicated by the central point in each curve, corresponding to $j = 0$, and they evolve according to the direction of the arrow in each curve. It is more apparent that the positive real part corresponds to the co-rotating modes and the negative to the counter-rotating ones. The former have an imaginary part that increases approaching zero; these frequencies correspond to those with a longer lifetime. In contrast, the imaginary part of the counter-rotating branch becomes smaller, causing the modes to be absorbed more quickly.

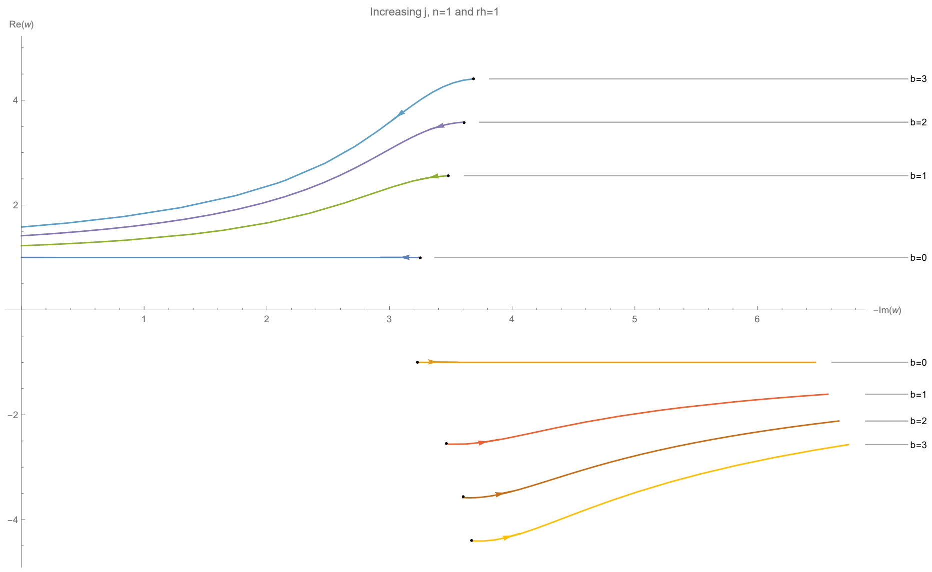

Figure 4.4.4: Fundamental mode frequency for curves with different values of the hair parameter b, angular momentum of the black hole j increasing from zero at the central points of each curve and evolving along the direction of the arrow. Furthermore, the radius of the event horizon $r_+ = 1$, the angular momentum of the scalar field $n = 1$ and the effective mass $m^2_{\text{eff}} = 4$ are fixed.

Chapter 5

Conclusion

Normal and quasi-normal modes were obtained in various geometries, employing analytical methods in some cases and numerical methods in others. Notably, novel results emerged from studying the propagation of a massless scalar probe over static solitons and rotating black holes, which are solutions to the Einstein-Gauss-Bonnet theory at the Chern-Simons point.

Starting with the soliton geometry, the observed normal modes exhibit a monotonic behavior when studying the variation of the gravitational parameter b, as illustrated in Figure 4.3.1. Conversely, when analyzing the behavior of the frequencies under a parametrization of the soliton size, an anomaly is observed for small values of the parameter $r_0/\sqrt[3]{b}$, as shown in Figure 4.3.2. As the soliton size decreases, corresponding to larger values of r_0, the frequencies are expected to increase, while otherwise they should be lower. However, a slight increase in frequency is observed for larger soliton sizes.

Quasi-normal modes for rotating black holes are first analyzed by setting $b = 0$, which reduces the geometry to the rotating BTZ black hole. This yields analytical results that provide us with the seed for further studies when the gravitational hair is not zero. Beginning with the search for fundamental modes, we fix the angular momentum of the scalar field to $n = 0$ for small values of the black hole angular momentum j while increasing b, as depicted in Figure 4.4.2. A distinctive behavior emerges: starting from the same value for the real part of the frequency and two values for the imaginary component differing only in sign, consistent with the analytical result, a critical value of b is reached. At this point, the real part of the frequency splits into two values differing in sign, while the imaginary components merge into a single value, resulting in modes with the same absorption rate.

To continue, frequencies are calculated for $n = 1$ while the angular momentum of the black hole increases, considering different curves where b is held fixed, as shown in Figure 4.4.4. The results indicate the same magnitude but opposite sign for the real part of the frequency, while the imaginary part remains. When the angular momentum of the field is nonzero, a co-rotating branch emerges, characterized by a longer lifetime, and a counter-rotating branch that is more heavily damped, approaching the real axis as the background geometry approaches extremality.

References

[1] B. P. Abbott, R. Abbott, T. D. Abbott, et al. (LIGO Scientific Collaboration and Virgo Collaboration), "Observation of Gravitational Waves from a Binary Black Hole Merger", Phys. Rev. Lett. **116**, 061102 (2016).
[2] M. Bañados, C. Teitelboim, and J. Zanelli, "Black hole in three-dimensional spacetime", Physical Review Letters **69**, 1849–1851 (1992).
[3] M. Abramowitz and I. A. Stegun, *Handbook of Mathematical Functions with Formulas, Graphs, and Mathematical Tables*, ninth Dover printing, tenth GPO printing (Dover, New York, 1964).
[4] G. T. Horowitz and V. E. Hubeny, "Quasinormal modes of AdS black holes and the approach to thermal equilibrium", Physical Review D **62**, 10.1103/physrevd.62.024027 (2000).
[5] A. Anabalón, D. Astefanesei, A. Cisterna, et al., "Rotating and accelerating AdS black holes in Einstein-Gauss-Bonnet Gravity", en, arXiv:2404.04691 [gr-qc, physics:hep-th] (2024).
[6] V. Cardoso and J. P. S. Lemos, "Scalar, electromagnetic, and Weyl perturbations of BTZ black holes: Quasinormal modes", Physical Review D **63**, 10.1103/physrevd.63.124015 (2001).
[7] A. Jansen, *Overdamped modes in Schwarzschild-de Sitter and a Mathematica package for the numerical computation of quasinormal modes*, 2017.

Appendix A

Numerical method

Below is the structure of the Mathematica code used, which was developed by Dr. Andrés Anabalón with modifications made by Dr. Julio Oliva, Monserrat Aguayo and Lilianne Tapia.

A1 Quasi-normal modes of BTZ black hole

The code shown below allows us to know the imaginary parts of the harmonics given the real part. In the one shown we have set $\mathrm{Re}(\omega) = 1$.

Listing A.1: Numerical method $\mathrm{Im}(\omega)$ BTZ black hole.

```
(*First the values of the constant terms are defined,*)
 {rmas = 1, m = 1, orden = 6}
(*then the power series *)
 R = 1 + Sum[a[i] z^i, {i, 1, orden}] + O[z]^(orden + 1)
(*The differential equation to be solved is entered as
 a function of x, to do this it is first necessary to
 change the variable to the radial coordinate r= 1/(1-x),*)
 Eq = -rmas^2*z*(z - 1)*D[R, z, z]
      + rmas*(z - 1)*(I*w - rmas)*D[R, z]
      + R*(-1/4*m^2 + 1/4*w^2)
 (*then*)
 Do[eqs[j] = SeriesCoefficient[Eq, j], {j, 0, orden}]
 {minusb, n} = CoefficientArrays[Thread[Array[eqs, orden, 0]
               == ConstantArray[0, orden]], Array[a, orden]]
```

```
 b = -minusb
(*Now the linear equations are solved for the eigenvalues.*)
 sol = LinearSolve[n, b, Method -> OneStepRowReduction]
 coefs = Thread[Array[a, orden] -> sol]
(*The power series is evaluated at each coefficient and the
 result is saved*)
 solu = 1 + Sum[a[i] z^i, {i, 1, orden}] /. coefs
(*Conditions are defined at the cut-off point*)
 bcsolu[w_] = N[solu /. z -> 1/10]
 Dbcsolu[w_] = N[D[solu, z] /. z -> 1/10]
(*The differential equation from the beginning is defined
 again but now writing the function to be solved as F[z].*)
 Equ[w_] = -rmas^2*z*(z - 1)*D[F[z], z, z]
          + rmas*(z - 1)*(I*w - rmas)*D[F[z], z]
          + F[z]*(-1/4*m^2 + 1/4*w^2)
(*Imposing initial conditions at the cut-off point for F[z],
 in addition to Dirichlet boundary conditions.*)
 SOL[w_] := Module[{bc, sys}, bc = {F[1/10] == bcsolu[w],
           F'[1/10] == Dbcsolu[w]};
           sys = {Equ[w] == 0, bc[[1]], bc[[2]]};
           NDSolve[ sys, F, {z, 1/10, 999/1000},
           AccuracyGoal -> 20, PrecisionGoal -> 20,
           WorkingPrecision -> 35]]
 SOL1[w_] := Evaluate[F[z] /. SOL[w]][[1]] /. z -> 0.999
(*Finally, the frequency w of the SOL1[w] function is
 plotted.*)
  Plot[{Re[SOL3[1 - iw*I]], Im[SOL3[1 - iw*I]]}, {iw, 0, 6},
  PlotRange -> {{0, 6}, {-0.01, 0.01}},
  AxesLabel -> {Im[w], "F(x^1)"}]
```

A2 Quasi-normal modes of Schwarzschild-AdS black hole

It is possible to numerically obtain the real and imaginary parts of this geometry with code using the ContourPlot package integrated into Mathematica.

Listing A.2: Numerical method QNM Schwarzschild-AdS black hole.

```
(*First the values of the constant terms are defined,*)
{rmas = 1, L = 0, l = 1, orden = 5}
(*then the power series *)
R = 1 + Sum[a[i] z^i, {i, 1, orden}] + O[z]^(orden + 1)
(*The differential equation for this case is derived by
following the steps described in Chapter 3, which leads to
an extended expression. Then*)
Do[eqs[j] = SeriesCoefficient[Eq, j], {j, 0, orden}]
{minusb, n} = CoefficientArrays[Thread[Array[eqs, orden, 0]
              == ConstantArray[0, orden]], Array[a, orden]]
b = -minusb
(*Now the linear equations are solved for the eigenvalues.*)
sol = LinearSolve[n, b, Method -> OneStepRowReduction]
coefs = Thread[Array[a, orden] -> sol]
(*The power series is evaluated at each coefficient and the
result is saved*)
solu = 1 + Sum[a[i] z^i, {i, 1, orden}] /. coefs
(*Conditions are defined at the cut-off point*)
bcsolu[w_] = N[solu /. z -> 1/10]
Dbcsolu[w_] = N[D[solu, z] /. z -> 1/10]
(*The differential equation from the beginning is defined
again but now writing the function to be solved as F[z].
Imposing initial conditions at the cut-off point for F[z],
in addition to Dirichlet boundary conditions.*)
SOL[w_] := Module[{bc, sys}, bc = {F[1/10] == bcsolu[w],
           F'[1/10] == Dbcsolu[w]};
           sys = {Equ[w] == 0, bc[[1]], bc[[2]]};
           NDSolve[ sys, F, {z, 1/10, 999/1000}]]
SOL1[w_] := Evaluate[F[z] /. SOL[w]][[1]] /. z -> 0.999
(*Finally, the frequency w of the SOL1[w] function is
plotted.*)
ContourPlot[Abs[SOL1[rw+I*iw]],{rw,4578/1000,45793/10000},
  {iw, -2554/1000, -25554/10000}, PlotPoints -> 50]
```

For each axis, we have considered an interval for the real and imaginary parts of the frequency based on the data presented in Table 1 of Reference [4].

A3 Quasi-normal modes of Einstein-Gauss-Bonnet theory at the Chern-Simons point

The following code allows us to analyze how a parameter affects the quasi-normal modes in a geometry, which is essentially the same as the one used above, but with modifications in the last lines.

Listing A.3: Numerical method QNM Einstein-Gauss-Bonnet at the Chern-Simons point

```
(* First the values of the constant terms are defined*)
 {j = 1/10, p = 0, kp = 0, kx = 0, cte = -(p + 4)*(p + 1),
  orden = 8}
(*then the power series *)
 R = 1 + Sum[a[i] z^i, {i, 1, orden}] + O[z]^(orden + 1)
(* The differential equation is introduced, which is a very
 extensive expression for this case, then  *)
 Do[eqs[j] = SeriesCoefficient[Eq, j], {j, 0, orden}]
 {minusb, n} =
    CoefficientArrays[
    Thread[Array[eqs, orden, 0] == ConstantArray[0, orden]],
    Array[a, orden]];
 v = -minusv
(*Now the linear equations are solved for the eigenvalues.*)
 sol = LinearSolve[n, b, Method -> OneStepRowReduction]
coefs = Thread[Array[a, orden] -> sol]
(*The power series is evaluated at each coefficient and the
 result is saved*)
 solu = 1 + Sum[a[i] z^i, {i, 1, orden}] /. coefs
(*It is then integrated into a for loop that requires an
 initial value, which can be obtained from the analytical
  expression since we start from b=0.*)
 For[u = 0; i = 1; t = -(19/20) (1 + Sqrt[5]) I, u < 1z,
 u = u + 1/1000; i = i + 1; t = w /.
 FindRoot[solu[w, u, 1], {w, t}, WorkingPrecision -> 10,
 PrecisionGoal -> 10], wj01[i] = t; rmasj01[i] = u]
(*The data is saved and finally graphed.*)
 b01 := Join[Array[rmasj01, i - 1]]
```

```
iw := Im[Join[Array[wj01, i - 1]]]
rw := Re[Join[Array[wj01, i - 1]]]
ListPlot[Transpose[{b01,-iw}],AxesLabel -> {"b",-Im[w]}]
ListPlot[Transpose[{b01, rw}],AxesLabel -> {"b", Re[w]}]
```